Available online at www.sciencedirect.com
SCIENCE DIRECT®

Journal of the European Ceramic Society 24 (2004) 2613–2617
www.elsevier.com/locate/jeurceramsoc

The effects of drying temperature on the crystallization of $YMnO_3$ thin films prepared by sol-gel method using alkoxides

Kyoung-Tae Kim, Chang-Il Kim*

School of Electrical and Electronic Engineering, Chungang University, 221, Huksuk-Dong, Dongjak-Gu, Seoul 156-756 South Korea

Received 15 April 2003; received in revised form 18 April 2003; accepted 21 April 2003

Abstract

In present work, we have investigated the structure and ferroelectric properties of the $YMnO_3$ thin films on Pt(111)/Ti/SiO_2/Si substrate fabricated by a sol-gel process using alkoxides. The crystal orientations and microstructures of the $YMnO_3$ thin films were investigated by X-ray diffraction (XRD), atomic force microscopy (AFM), and scanning electron microscopy (SEM). The preferred c-axis orientation and the dielectric characteristics of $YMnO_3$ thin films were improved by increasing the drying temperature. The ferroelectric properties such as remanent polarization were found to be dependent on the orientations of the $YMnO_3$ thin films. As a result, the highly c-axis oriented $YMnO_3$ thin films exhibited higher remanent polarization ($2Pr = 3.6\ \mu C/cm^2$) compared with randomly oriented $YMnO_3$ thin films. The dielectric constant of thin film dried at 450 °C is 19 that is close to $YMnO_3$ single crystal. It was found that the higher drying temperature affects the ferroelectric properties due to higher crystallinity with the c-axis preferred orientation.

Keywords: Dielectric properties; Drying; Ferroelectric properties; Thin films; Sol-gel process; $YMnO_3$

1. Introduction

Ferroelectric random access memory (FRAM) has attracted much attention for next generation memory devices because of the nonvolatile operation and high access speed.[1,2] FRAMs are classified into destructive readout (DRO) and nondestructive readout (NDRO) type. NDRO metal-ferroelectric-semiconductor field-effect transistors (MFSFET) have the noticeable advantages such as small cell size and simple structure.[3–5] In the MFSFET structure, it is necessary to provide form a good interface of ferroelectric thin films with Si and to obtain a relatively low permittivity.[6,7]

Generally, the ferroelectric materials for FRAMs are classified into Pb-containing group such as $PbTiO_3$ (PT), $Pb(Zr,Ti)O_3$ (PZT), $(Pb,La)(Zr,Ti)O_3$ (PLZT) and Bi-containing group such as $Bi_4Ti_3O_{12}$ (BTO), $SrBi_2Ti_2O_9$ (SBT) etc. However, the ferroelectric materials mentioned above easily form a point defects because of the high volatility of both Pb and Bi, which diffuse easily into the Si substrates. On the other hand, the ferroelectric $YMnO_3$ thin films are expected to be more suitable dielectric material for MFSFET structures due to the absence of volatile components. Moreover, the $YMnO_3$ thin films have a relatively low permittivity ($\epsilon_r = 20$) and a single *c*-axis polarization.

Until now, there are several works reported about $YMnO_3$ thin films deposited using methods such as molecular beam epitaxy (MBE), pulsed laser deposition, RF-sputtering, and sol-gel method.[8–11] Nevertheless, the systematic investigations about the influence of the deposition process parameters on the ferroelectric properties are absent.

In this study, the $YMnO_3$ thin films were prepared by the sol-gel method together with spin-coating technique. The effect of drying temperature on the crystallization of the films was investigated. The crystallographic orientation of the films was investigated using X-ray diffraction (XRD). The microstructures of the films $YMnO_3$ were studied using atomic force microscopy (AFM) and scanning electron microscopy (SEM). The electrical properties of $YMnO_3$ thin films were investigated using a precision workstation and a LF impedance analyzer.

* Corresponding author.
E-mail address: cikim@cau.ac.kr (C.-I. Kim).

0955-2219/$ - see front matter © 2003 Elsevier Ltd. All rights reserved.
doi:10.1016/j.jeurceramsoc.2003.08.010

2. Experimental

For the preparation of $YMnO_3$ precursor, $Y(CH_3CO_2)_3{\cdot}xH_2O$ (yttrium acetate hydrate, 99.9%, Aldrich. Co.) and $Mn(CH_3CO_2)_2{\cdot}4H_2O$ (manganese(II) acetate tetrahydrate, 99.9%, Aldrich. Co.) were dissolved in 2-methoxyetanol separately and refluxed at 125 °C for 3 h. The solutions were mixed with a molar ratio of Y: Mn = 1: 1. The mixed solution was refluxed for 2 h at 70 °C and then distilled at 125 °C for 5 h. Finally, the distilled water and acetylacetone were added to a 0.15 M $YMnO_3$ stock solution and the solution was refluxed.

The $YMnO_3$ films were deposited onto the Pt(111)/Ti/SiO_2/Si(001) substrate (MFM-type) or Si substrate (MFS-type) using the spin-coating method. The spinner operated at 4000 rev./min for 30 s. The thermal treatments were performed for 10 min on the hot plate under the various drying temperature ranging from 300 to 450 °C. A detailed schematic diagram of the sol-gel method is shown in Fig. 1. The coating and thermal treatments were repeated 7 times to obtain a final thickness of 300 nm. After the spin-coating, the films were finally annealed at 850 °C in ambient O_2 for 1 h. The dielectric measurements were carried out in the MFM and MFS structure capacitor. For electrical measurements, the top electrodes of 300 μm diameter were fabricated by depositing the 150-nm-thick Pt film at room temperature using dc magnetron sputtering. The powder precusors were examined by thermogravimetric analysis (TGA)/differential scanning calorimetry (DSC). The crystallographic orientations of the films were investigated using XRD (Rigaku-D/MAX diffractometer with CuK_α emission). The surface morphologies of the films were examined using AFM (PSI). The cross-sectional microstructures of the films were observed using a JEOL 6330F field emission scanning electron microscope (FE-SEM). The ferroelectric properties of $YMnO_3$ films were examined using the precision workstation ferroelectric tester (Radiant Technologies, USA). The dielectric constant and loss were measured using an HP 4192 impedance analyzer. The leakage current densities of $YMnO_3$ thin films were measured using a HP 4146C semiconductor parameter analyzer at conditions of 0.1-V step voltage and delay time of 20 s.

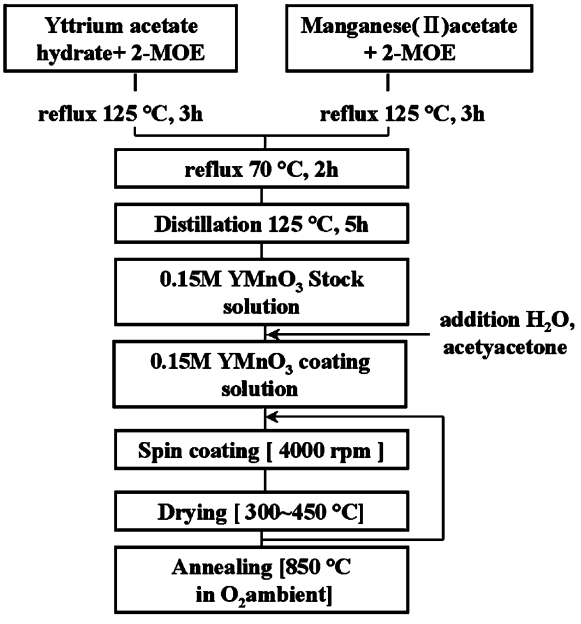

Fig. 1. The flow diagram for preparing $YMnO_3$ thin film by sol-gel method.

3. Results and discussion

Fig. 2 shows the DSC and TGA curves of the dried $YMnO_3$ powder. The experimental conditions providing these data may be described as follows. The precusor solution was dried at 80 °C for 24 h. After drying, the $YMnO_3$ powders were heated slowly 10 °C/min up to 1000 °C under air atmosphere. The weight loss of the dried powder was about 21.2% at 1000 °C, as determined by the TGA curve. The data of Fig. 2 indicates the decomposition of dried powder includes three steps: (a) removing the hydrated water between room temperature and 160 °C, (b) the combustion of residual organic compounds between 160 and 400 °C, and (c) the formation of $YMnO_3$ by the decomposition of intermediate carbonate between 650 and 700 °C.

Fig. 3 represents the XRD patterns of $YMnO_3$ thin films prepared under various drying temperatures. All the films show hexagonal phases, but no secondary phases were observed. The peak intensity of (0004) from the hexagonal phase increases slowly as the drying temperature increases to 400 °C. However, the *c*-axis (0004) peak is not dominant below 400 °C. The $YMnO_3$ thin films that were dried below 400 °C showed typical XRD patterns of polycrystalline structure without the

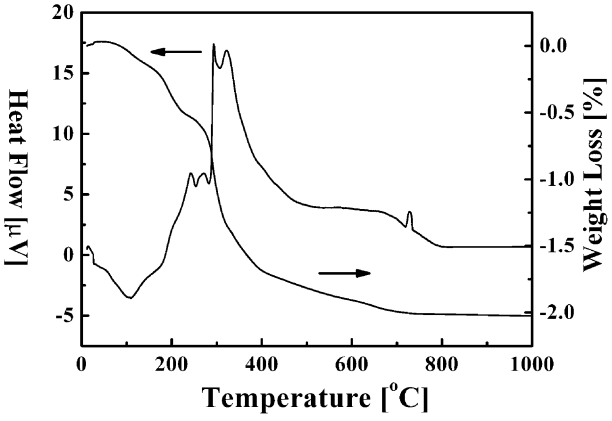

Fig. 2. DSC/TGA curves of the dried $YMnO_3$ powders.

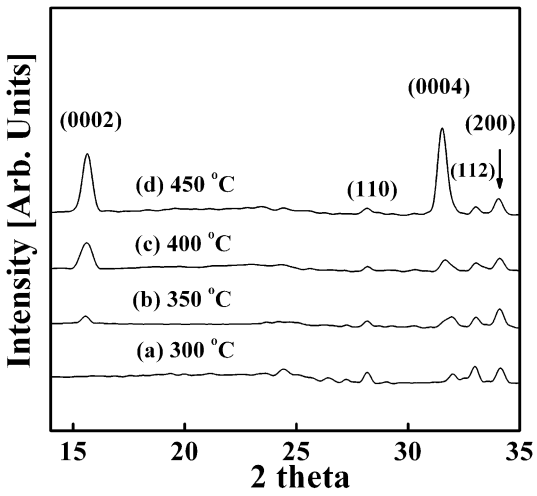

Fig. 3. XRD patterns of $YMnO_3$ thin films as function of drying temperatures.

preferred orientation. As the drying temperature increases more than 450 °C, the peak intensity of (0004) increased rapidly and (0002) peak appears. The (112) peak intensities decrease with the increasing drying temperature. The effect of drying temperature may be probably related to the different growth of oriented structure. However, to determine the exact mechanism of the influence of drying temperatures on the orientation of $YMnO_3$ thin films, additional investigations are need. To quantify the *c*-axis orientation of the films, the equation $\alpha = I(0004) / [I(0004) + I(112)]$ was used.[12] In this equation, the α is a definition of relative peak intensity for (0004) direction. The calculations showed that the value of α increases proportionally to the increases of the drying temperature. Considering the data of Fig. 2, the corresponding α is 0.37, 0.47, 0.65 and 0.86. This indicates that the drying temperature below 350 °C is insufficient to obtain high *c*-axis orientation. The reason for this phenomenon may be assumed as follows. The (0001) plane in a hexagonal close packed (hcp) crystal has the same symmetry as the {111} plane in a cubic crystal. When the samples were dried on the hot plate, the adatoms on Pt (111) substrate diffused along the close packing direction of low surface energies for geometrical compact formation. It is suggested that the growth of the drying temperatures increases the mobility of atoms on the Pt (111) substrate, providing the favorable conditions for nucleation of hexagonal $YMnO_3$ that improve the crystallinity of films to preferred *c*-axis orientation.

Fig. 4 shows the surface morphologies of $YMnO_3$ thin films prepared in the range of drying temperature from 300 to 450 °C. As the drying temperature increases, the surface roughness also increases. The grain size changes from 60 to 120 nm as the drying temperature changes between 300 and 450 °C. All the AFM images show uniform microstructure and low surface roughness (~5 nm). Therefore, all the films generally have good microstructure with few defects such as pinholes or microcracks. Crack free surface is an important feature because the cracks resulted from film stress affect the dielectric loss.[9] Additionally, it is important to note that the surface roughness of the films increases with the increasing drying temperature. We assume this effect to be the results of the grain growth.

Fig. 5 shows the cross-sectional SEM images of $YMnO_3$ thin films dried at 450 °C. As can be seen in the cross-sectional micrograph, this film consists of fine grains with submicron size. The surface is relatively flat,

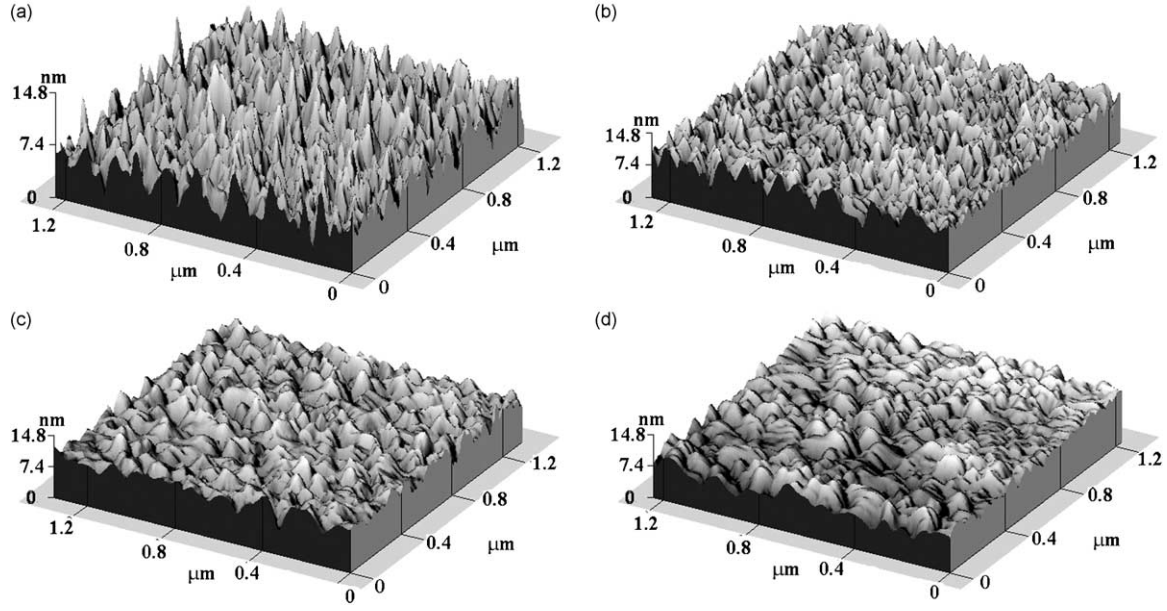

Fig. 4. AFM images of $YMnO_3$ thin films dried at (a) 300 °C, (b) 350 °C, (c) 400 °C, and (d) 450 °C as function of drying temperatures.

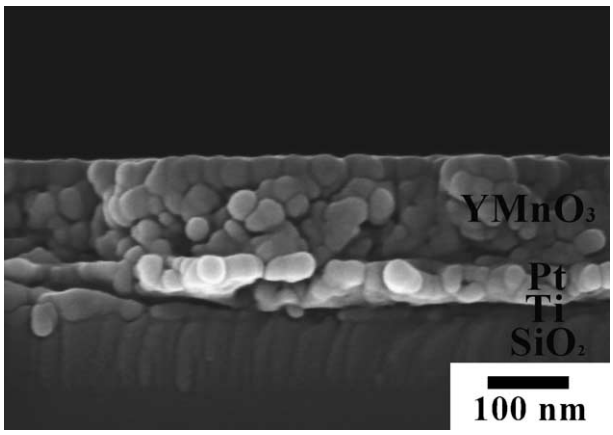

Fig. 5. Cross-sectional SEM images of $YMnO_3$ thin films dried at 450 °C.

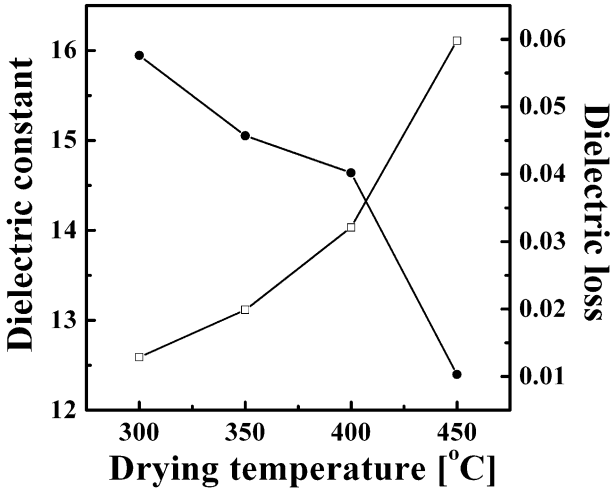

Fig. 6. (a) Dielectric constant and dielectric loss of $YMnO_3$ thin films as function of drying temperatures measured at 100 kHz.

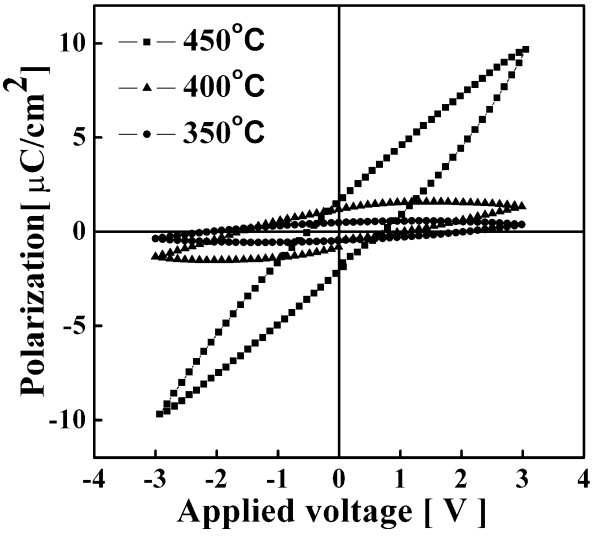

Fig. 7. P-V hysteresis curves of $YMnO_3$ thin films prepared with drying temperature of 350, 400, and 450 °C.

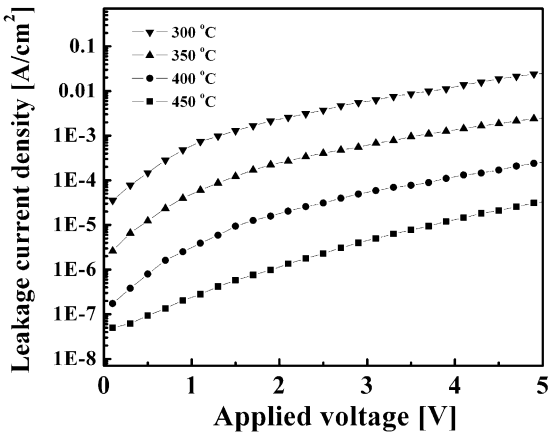

Fig. 8. Leakage current densities of $YMnO_3$ thin films as function of drying temperatures and applied voltage.

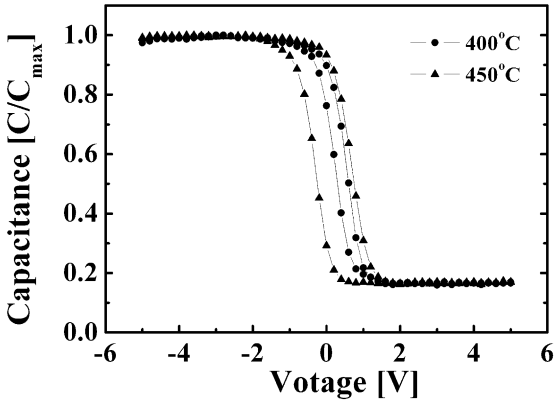

Fig. 9. Capacitance-voltage characteristic of $Pt/YMnO_3/Si$ structure dried at 400 and 450 °C.

and the thickness of the films is about 300 nm. The data of Fig. 5 reveal the dense microstructure with uniform thickness and the absence of significant reaction between the thin film and Pt electrodes.

Fig. 6 shows dielectric constant and dielectric loss of $YMnO_3$ thin films as a function of drying temperature measured at 100 kHz. Dielectric constants were calculated by measuring the MFM structure. It can be seen that the increases of drying temperature causes the increase of dielectric constant. As the results, the $YMnO_3$ thin film dried at 450 °C has the highest dielectric constant of 19. This value is a very close to the value for hexagonal $YMnO_3$ single crystal ($\epsilon_r = 20$). As the same time the dielectric loss decreases rapidly as the drying temperature increases. We assume that the differences of dielectric losses for the various drying temperatures may be related to structural changes such as grain sizes and crystal orientations. The excessive dielectric loss of $YMnO_3$ is the possible reason for the lack of a ferroelectric hysteresis property. Considering all the results discussed above we propose that the improvement of ferroelectric properties compared with the randomly oriented $YMnO_3$ films results from the

improvement of crystal structure such as prepared *c*-axis orientation.

Fig. 7 shows the P-V characteristic of a Pt/$YMnO_3$/Pt (111) capacitor prepared as a function of drying temperature. Although all the P-V curves exhibit a hysteresis loop, the remanent polarization (2Pr) has a maximum value of about 3.6 μC/cm^2 for the drying temperature of 450 °C. For the drying temperatures below 450 °C, the ferroelectric properties of films are very poor. This fact may be attributed to worse crystallization and smaller grain size compared with the films dried at 450 °C. Fig. 7 shows also that the hysteresis loop for the films dried at 400 °C is bulged. The probable reason is the increasing of the leakage current.

Fig. 8 shows the leakage current densities of $YMnO_3$ thin films dried at various temperatures as a function of applied field. The previous investigations reported that the leakage current properties of ferroelectric thin films depend upon the thin film deposition method, composition, annealing temperature, electrode, microstructure, film thickness, and surface roughness.[13] As the drying temperature of $YMnO_3$ thin film increases from 350 to 450 °C, the leakage current density of the $YMnO_3$ thin films decreases. We assume that lower leakage current may be caused by the higher crystallinity and *c*-axis orientation of the $YMnO_3$ thin film. The detailed leakage current mechanisms of the $YMnO_3$ thin films will be published elsewhere. The lower leakage current density corresponding to the $YMnO_3$ thin film dried at 450 °C is 2.82×10^{-7} A/cm^2 at 1 V.

Fig. 9 shows the 1 MHz C-V characteristics of Pt/$YMnO_3$/Si structure dried at 400 and 450 °C, respectively. The applied voltage was changed 0.2 V/s from +5 V to −5 V and from −5 V to +5 V. As the drying temperature increased, the memory window for the $YMnO_3$ thin films increases. We attributed this result to the behavior of ferroelectric remanent polarization, which increases as the maximum applied voltage increases. The results mentioned above also affect the observation of the ferroelectricity at room temperature of the MFS structure. As shown in Fig. 8, the memory window of the $YMnO_3$ thin film dried at 450 °C was about 1.03 V.

4. Conclusion

We deposited $YMnO_3$ thin films on the Pt(111)/Ti/SiO_2/Si and Si (100) substrates by sol-gel process using alkoxides. The $YMnO_3$ thin films spun-coated and dried on hot plates from 300 to 450C. The prepared $YMnO_3$ thin films were annealed at 850 °C in O_2 atmosphere for 1 h. From the result of XRD, AFM and SEM analysis, the crystallization of $YMnO_3$ thin films improve to preferred orientation by increasing the drying temperature. Ferroelectric properties such as remanent polarization were found to be dependent on the orientation of the $YMnO_3$ thin films. As a result, the highly *c*-axis oriented $YMnO_3$ thin films exhibited higher remanent polarization (2Pr = 3.6 μC/cm^2) compared with randomly oriented $YMnO_3$ thin films. From these results, it is suggested that appropriate increment of drying temperature improves the crystallization for preferred orientation by enhancing the creation of nucleation sites of hexagonal $YMnO_3$.

References

1. Scott, J. F. and Araujo, C. A., Ferroelectric memories. *Science*, 1989, **246**, 1400–1405.
2. Parker, L. H. and Tasch, A. F., Ferroelectric materials for 64 Mb and 256 Mb DRAMs. *IEEE Circuits Device Mag*., 1990, **6**, 17–26.
3. Rokuta, E., Hotta, Y., Tabaa, H., Kobayashi, H. and Kawaki, T., Low leakage current characteristics of $YMnO_3$ on Si(111) using an ultrathin buffer layer of silicon oxynitride. *J. Appl. Phys*., 2000, **88**, 6598–6604.
4. Yoon, S. M., Tokumitsu, E. and Ishiwara, H., Realization of adaptive learning function in a neuron circuit using metal/ferroelectric ($SrBi_2Ta_2O_9$)/semiconductor field effect transistor (MFSFET). *Jpn. J. Appl. Phys*., 1999, **38**, 2289–2293.
5. Kim, K. H., Metal-ferroelectric-semiconductor (MFS) FET's using $LiNbO_3$/Si (100) structures for nonvolatile memory application. *IEEE Electron Device Lett*., 1998, **19**, 204–206.
6. Alexe, M., Kastner, G., Hesse, D. and Gosele, U., Ferroelectric-semiconductor heterostructures obtained by direct wafer bonding. *Appl. Phys. Lett*., 1997, **70**, 3416–3418.
7. Mou, D., Petterson, C. S., Linnros, J. and Rao, K. V., Fabrication and properties of metal/ferroelectrics/semiconductor diodes on 4H-SiC. *Appl. Phys. Lett*., 1998, **73**, 1532–1534.
8. Imada, S., Kuraoka, T., Tokumitsu, E. and Ishiwara, H., Ferroelectricity of $YMnO_3$ thin films on Pt(111)/Al_2O_3(0001) and Pt(111)/Y_2O_3(111)/Si(111) structures grown by molecular beam epitaxy. *Jpn. J. Appl. Phys*., 2001, **40**, 666–671.
9. Cho, S. H., Song, J. H., Lee, K. B. and Jeong, T. H., Structure and ferroelectric properties of $YMnO_3$ thin films deposited on platinum electrodes. *J. Korean Phys. Soc*., 1999, **35**, S1251–S1255.
10. Lee, H. N., Kim, Y. T. and Park, Y. K., Memory window of highly c-axis oriented ferroelectric $YMnO_3$ thin films. *Appl. Phys. Lett*., 1999, **74**, 3887–3889.
11. Kitahara, H., Tadanaga, K., Minami, T., Fujiura, N. and Ito, T., Lowering the crystallization temperature of $YMnO_3$ thin films by the sol-gel method using an yttrium alkoxide. *Jpn. J. Appl. Phys*., 1999, **38**, 5448–5451.
12. Song, Z., Fu, X., Gong, J. and Lin, C., A study on microstructure and electrical properties of $Pb_{0.8}La_{0.1}Ca_{0.1}Ti_{0.975}O_3$ thin films prepared by metal-organic decomposition. *Jpn. J. Appl. Phys*., 1999, **38**, 6415–6420.
13. Horwitz, J. S., Chang, W., Carter, A. C., Pond, J. M., Kirchoefer, S. W., Chrisey, D. B., Levy, J. and Hubert, C., Structure/property relationships in ferroelectric thin films for frequency agile microwave electronics. *Integr. Ferroelectr*., 1998, **22**, 279–289.